# ANALYSIS OF VISCOUS FINGERING REPRODUCIBILITY IN CONSOLIDATED NATURAL POROUS MEDIA

Arlindo da Costa e Silva, Petrobras/Cenpes

## Abstract

The purpose of this work is to apply computerized X-Ray tomography techniques to visualize the development of viscous fingering during the displacement of an oil phase through an homogeneous, natural and consolidated porous media.Viscous fingering during two-phase flow is obtained by appropriate selection of both injection rate and mobility ratio.

The porosity and saturation profiles have been computed by means of image analysis through the use of a graphical interpretation software. The image analysis of the cross sections shows that, under conditions of hydrodynamic stability, the displacement of water by oil occurs as predicted by the piston-like model, with small gravitational effects. On the other hand, when the oil phase is displaced by a water phase under unstable hydrodynamic conditions, the injected water flows through well defined regions of the porous media. Gravity segregation is also observed in this case.

Provided the injection parameters and the connate water saturation are kept constant, the water saturation profiles as a function of self-similar dimensionless variable ($x_D$ / $t_D$ ) merge to a single curve. For the same injection conditions, it was observed that the curves of oil permeability *versus* water saturation overlap themselves. Such overlapping also happens with the water relative permeability *versus* water saturation curves. It was evident that the oil relative permeabilities are strongly influenced by the injection rate of a higher mobility fluid.

The shape of the water relative permeability curves indicates the existence of two different displacement mechanisms taking place along the core. Moreover, the water fractional flow curve is characteristic of unstable displacement.

## Introduction

When a fluid displaces a more viscous fluid, the displacement front may become unstable, resulting in viscous fingering. Apart from reducing the displacement efficiency, instability may invalidate the usual method of simulating immiscible displacement performance based on relative permeability and capillary pressure concepts. Therefore it would be beneficial to predict the possibility of fingering development as a factor in a waterflood project. Many stability studies of immiscible displacement have been reported in the literature with concerns to mobility ratio [1,2] , displacement velocity [3] , gravity and capillary forces [4,5] , rock permeability [6] , dimensionless scaling groups[7,8] and the visualization of displacements by CT images[9-14] . Peters *et alii* [7] showed that unstable immiscible displacements are self-similar processes and, when presented as a function of the self-similar dimensionless variable, the spatial and temporal saturation data collapses into one unique dimensionless response curve, so called response function.

The objective of this study was to perform several immiscible waterfloods under a pre-defined set of displacement condictions in order to verify the reproducibility of displacements. The corefloods were imaged by Computed Tomography (CT) to obtain their saturation distribution in time and space. This paper presents the dimensionless response curves of the experiments and relative permeability and fractional flow curves as well.

## Experimental Equipment and procedure

The porous media used in this study are cylindrical Vosges sandstones cores, a natural and consolidated outcrop obtained from the southern Rhinegraben, France. The Sample #1 has dimensions of 233.15 mm length and 54.12 mm diameter, average porosity of 0.227 and absolute permeability of

417 mD. The Sample #2 has dimensions of 233.0 mm length and 54.53 mm diameter, average porosity of 0.230 and absolute permeability of 497 mD.

Both samples were conceptually divided into 23 adjacent slices of 10 mm each, as shown by figure 1. Preliminary petrophysical experiments (capillary pressure, photomicrographies of thin layer and relative permeabilities) showed that these samples were very homogeneous in a macroscopic scale and strongly water-wet.

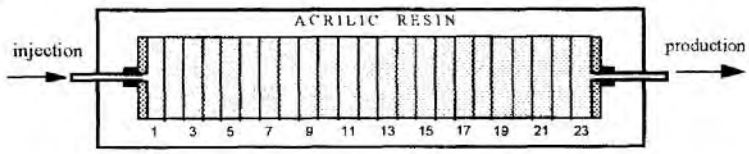


Figure 1 : Conceptual slices of the core samples

Viscous fingering during the immiscible displacement was obtained by appropriate selection of both injection rate and mobility ratio. The waterfloods were conducted at constant rates using a waters positive displacement pump. The displacing fluid was a 0.8 M potassium iodode solution with viscosity of 0.823 cP and density of 1.0962 g/cm$^3$ and the displaced fluid was a mineral oil .with viscosity of 244 cP and density of 0.8836 g/cm$^3$

An unmodified third generation CAT scanner ( GE CT-9800 scanner ) was used to obtain the fluid saturation distribution along the core. The general layout of the equipment used in experiments is shown in figure 2. The core was initially evacuated and then filled completely with a 0.8 M potassium iodide solution to provide an appropriate contrast to that of the oil. This aqueous phase was then displaced by the oil phase until irreducible water saturation (Swi). The core was placed in the CAT scanner and the displacing fluid (0.8 M KI solution) was injected into the core at a constant rate. At selected times following introduction of the displacing fluid, several contiguous scans (up to 14) were made at adjacent radial slices of the core. These scans can be stacked together to create a three-dimensional image of the water fingering so that we can monitor its advancing front. The images for this displacement were taken as radial cross-sections 10 mm wide. The time required for a complete scan was about 2 seconds and the gap of time between two sequencial scans was about 3 seconds. The computer unit computes local X-Ray attenuation coefficients over the scanning cross-section for pixels of 0.3125 x 0.3125 mm. The thickness of the element is equal to the width of the X-Ray beam (10 mm). These average X-Ray attenuation coefficients result from linear combination of the silica rock formation, oil and potassium iodide solution that occupy the pore spaces.

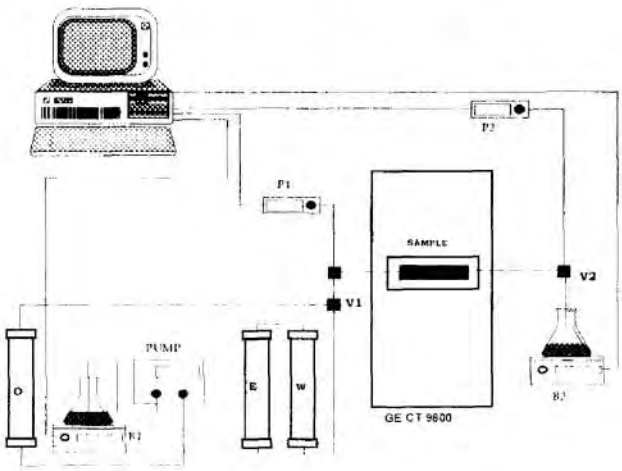


| | |
|---|---|
| PUMP | Waters positive displa-cement pump |
| B1,B2 | Semi-analytical digital ba-lances |
| P1,P2 | Pressure transducers |
| V1,V2 | Three-way valves |
| O | Oil vessels |
| E | Oil-cushion vessel |
| W | 0.8 M KI solution vessel |
| GE CT 9800 | Third-generation CAT scanner |

Figure 2 - Layout of experimental equipment

The rates of produced oil and water were computed from mass rate and fluid densities data. The amount of oil and water recovered was collected by a calibrated graduated cylinder placed in upside-down position and recorded as a function of time. A computer aided data acquisition system was assembled to monitor the waterflood and acquire mass rates (B1, B2), time and pressure data (P1, P2) as functions of time, as shown in fig. 2. The first experiment on sample #1 was conducted at constant flow rate of 0.5 $cm^3$/min. while all the other seven experiments (carried out on both sample #1 and #2) were conducted at constant flow rate of 0.3 $cm^3$/min. in order to investigate the influence of the velocity of the displacing fluid on the development of viscous fingering.

The image of each slice consists of a matrix of 256 x 256 pixels. These data are stored on magnetic media as CT numbers, proportional to the local X-Ray attenuation coefficients. These data were transferred to a SUN workstation on which all subsequent processing was done. The porosity and saturation profiles have been computed by means of image analysis through the use of a graphical interpretation software. These data are presented as color-filled maps of 179 x 179 pixels, along radial planes of the core.

## Determination of porosity and fluid saturation

The porosity and the fluid saturation at a voxel can be determined by solving the following simultaneous equations for each voxel [11].

$$S_W + S_O = 1 \quad (1)$$

$$\Psi m\,(1-\Phi) + \Psi_A\,\Phi = \Psi_{RA} \quad (2)$$

$$\Psi m\,(1-\Phi) + \Psi_W\,\Phi = \Psi_{RW} \quad (3)$$

$$\Psi m\,(1-\Phi) + (\Psi_W S_W + \Psi_O S_O)\,\Phi = \Psi_{RWO} \quad (4)$$

Since there are four equations and four unknown variables ( Sw, So, $\Psi m$ and $\Phi$ ), it is possible to determine the unique solution for the unknowns. Six CT scans are required as follows : Scan of an empty test cell, of a test cell filled with the KI solution, of a test cell filled with the mineral oil, of dry core, of core completely saturated with potassium iodide solution and of core saturated with the displaced and displacing fluids to determine $\Psi_A$, $\Psi_W$, $\Psi_O$, $\Psi_{RA}$, $\Psi_{RW}$ and $\Psi_{RWO}$ respectively. The first three scans are performed only as one cross-section of the test cell in order to obtain the average CT numbers of the fluids air, KI solution and mineral oil, respectively. The other three last scans are performed at all conceptual slices of the sample to determine the porosity and saturation profiles along the core. Solving equations 1 through 4 simultaneously, it can be shown that the porosity and the mineral oil saturation of each voxel are given by :

$$\Phi = \frac{\Psi_{RW} - \Psi_{RA}}{\Psi_W - \Psi_A} \quad (5)$$

$$S_O = \frac{\Psi_{RW} - \Psi_{RWO}}{\Phi\,(\Psi_W - \Psi_O)} \quad (6)$$

## Image Artifacts

Image artifacts are features in the processed image that are produced entirely by the imaging process but are not present in the original object. The most noticeable and damaging of those phenomena responsible for image artifact is beam hardening which produces an image with high attenuation coefficients around the periphery and low attenuation coefficients in the center of the object. A methodology for beam hardening correction[11] was applied in order to minimize the image artifact. All the porosity maps presented a concave profile with higher values around the periphery and lower values in the center of the core. Such porosity profiles did not match the ones expected for the core because, since the porous media is very homogeneous their porosity profiles should be somewhat flattened. The results of such correction are shown in table 1.

Figure 3 shows a series of gray-scaled porosity maps from contiguous slices of sample #2. Darker regions indicate higher porosity. One can see by the tomograms that the porosity is evenly distributed

within slices 11 to 14 with values ranging from 0.225 up to 0.235. Such regular porosity distribution also occur in the first 10 one-centimeter-slices of the sample #2. Nevertheless, in the slices closer to the production face the heterogeneity becomes higher. As we can see by the images of slices 19 and 20, there are regions of porosity as low as 0.085 and others of porosity as high as 0.290. The porosity profile of sample #1 did not show such high heterogeneities as sample #2 did. The porosity of sample #1 varied within a close range from 0.212 up to 0.235, with very small spots of higher porosity.

TABLE 1
Results of the Beam Hardening Correction

| Description | Sample #1 | Sample #2 |
|---|---|---|
| Porosity (conventional method) | 0.227 | 0.230 |
| CT porosity (before correction) | 0.244 | 0.249 |
| CT porosity (after correction) | 0.227 | 0.232 |
| Swi ( material balance) | 0.175 | 0.171 |
| CT Swi ( before correction ) | 0.196 | 0.190 |
| CT Swi ( after correction ) | 0.169 | 0.169 |

Figure 4 shows gray-scaled fluid saturation maps of the displacement of KI solution by the mineral oil after injection of 0.088, 0.174 and 0.390 pore volumes of mineral oil in sample #2. Darker gray indicates the advancing front of the injecting oil while light gray denotes the regions 100 % saturated by the aqueous phase.

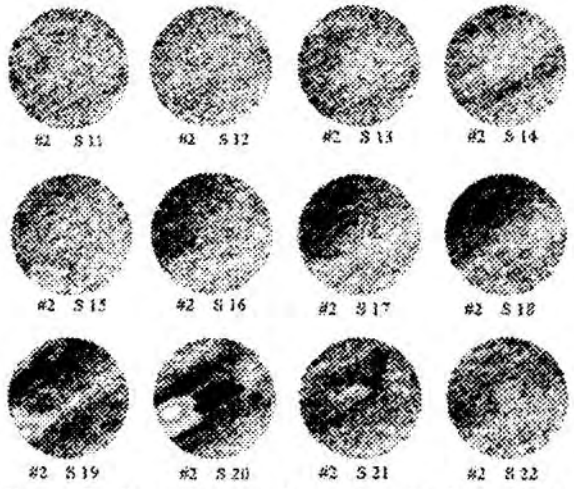


Figure 3 - Porosity maps from slices 11 through 22 of sample #2.

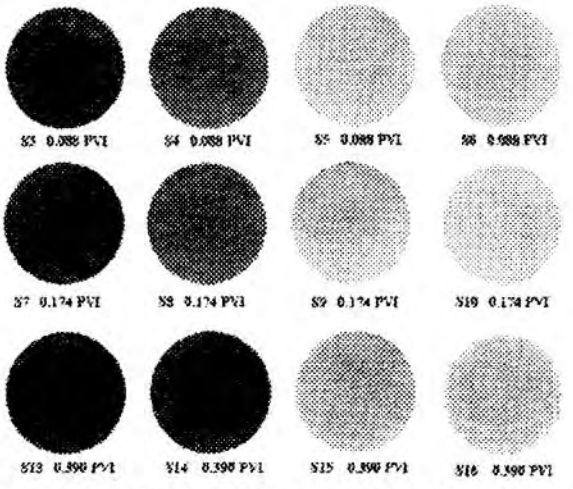

Figure 4 : Fluid saturation profiles from the oil injection in sample #2 at 3 times.

Considering that the displacement of water by oil takes place under conditions of hydrodynamic stability any eventual fingering should be due to channeling instead of viscous instability. Thus, scanning of the oil injection experiment attempted to identify channels of higher permeability should any exists in the core. The tomograms showed that the displacement of water by oil occurred as predicted by the piston-like model revealing the non-existence of channels of markedly higher permeability. Therefore, any development of fingering during the waterfloods, which are conducted under unstable hydrodynamic conditions, should be attributed to viscous instability only.

## Resaturation of samples

After the laboratory experiments the samples were resaturated to their initial fluid saturation condition, i.e. saturated by the mineral oil @ Swi. The resaturation procedures for sample #1 and sample #2 were different. For sample #1, after the waterflood both aqueous and oil phases were extracted by solvents. Then, the core was dried , saturated with KI solution and this aqueous phase was displaced by the mineral oil until Swi. For sample #2, after the waterflood, the injected water was again displaced by the mineral oil until no more water has been produced. The usage of the two different procedures of resaturation was aimed at verifying the influence of solvent cleaning on rock properties.

## Results and discussion

Four unstable immiscible displacements were carried out on each sample. Figures 5 through 8 show a comparison of radial saturation maps of four contiguous slices among the four experiments run on sample #2. In these figures the first down to the fourth lines are related to the first to the fourth waterfloods, respectively. In each figure the scans were taken after injection of, approximately, the same volume of KI solution. For the third experiment, the sample #2 was placed in the scanner, in the upside-down position in order to investigate the influence of gravity forces on the development of viscous fingers. By the use of specific routine for image rotation of the Khoros System, the images from the third waterflood went through a rotation of 180°. Thus, the pixels of the saturation maps presented at the third line of figures 5 through 8 are in the same spatial position as the other three lines.The light-gray areas indicate the regions already swept by the injected water. The fluid saturation profile of the first, second and fourth waterflood are quite similar i.e. the regions of the core preferentially invaded by the water are the same in these three saturation maps. However, when these three saturation profile are compared with the one took from the third waterflood, some differences stand out among them as follows :

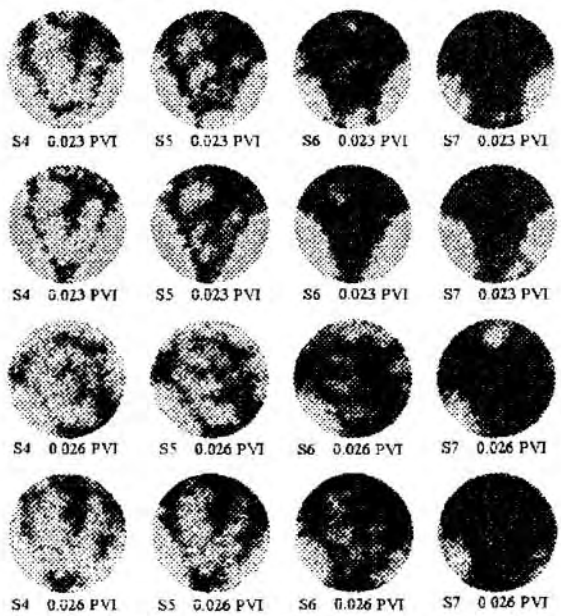


Figure 5 : Saturation maps of slices 4 through 7 from the waterfloods on sample #2

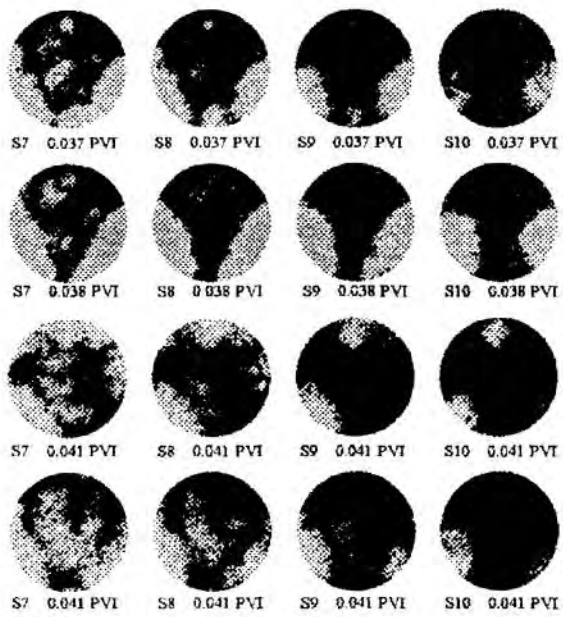


Figure 6 : Saturation maps of slices 7 through 10 from the waterfloods on sample #2

a) There was a fingering that have always appeared at the lower-left side of the core no matter the position the sample was placed in the scanner. It suggests that this fingering occurred in that region due

to some positive gradient of permeability. This supposed gradient of permeability must be of a minimal magnitude since the oil injection was not sensitive to it. The sand grains deposition planes may be assigned as a very probable cause for such low-scale heterogeneity.

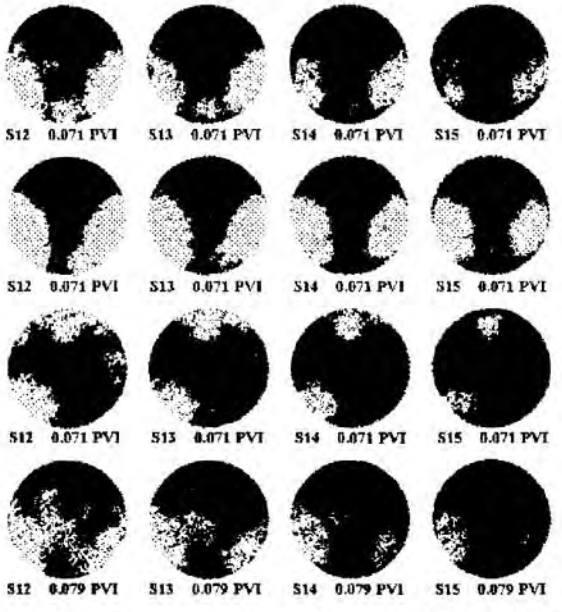


Figure 7: Saturation maps of slices 12 through 15 from the waterfloods on sample #2

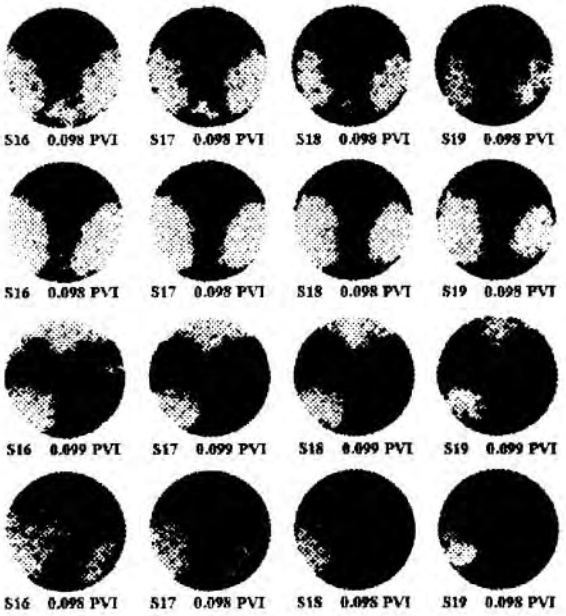


Figure 8: Saturation maps of slices 16 through 19 from the waterfloods on sample #2

b) There was a fingering that appeared in the lower-right side of the core in the first two waterfloods. This fingering was not observed anymore when the core was placed in the scanner rotated by 180°. Instead, we notice that another fingering appeared at the botton of the core during the third displacement. Moreover, for the fourth experiment, when the sample was placed in its original position again, the regions of development of fingering repeated the same configuration observed in the first two experiments.

These remarks were also observed for the experiments carried out on sample #1[11]. The images of the three displacements conducted under the same conditions showed similar configuration of fingering areas. Neverthless, when the sample #1 was turned upside-down, this configuration changed altogether. Such behaviour shows the strong influence that gravity forces and even minimal heterogeneities exert over fingering in sandstones core. It indicates that the fingering phenomena on natural and consolidated porous media may be understood as a deterministical and reproducible phenomena instead of a statistical one.

Figures 9 through 12 show the saturation data as a function of the dimensionless self-similar variable $x_D / t_D$. We can see that the saturation data collapse into one unique dimensionless response curves ($\mathbf{f}_{1D}$) that is characteristic of each unstable displacement [7].

The overlapping of the four dimensionless response curves suggests that the four displacements have quite identical characteristics what may mean reproducibility. The almost negligible discrepancies among the response curves may be due to the differences of connate water saturation of each experiment. If those experiments had been conducted under a given connate water saturation the response curves would have been the same. For the displacements carried out on sample #1[11], these discrepancies were somewhat coarser since the connate water saturation data were more spread.

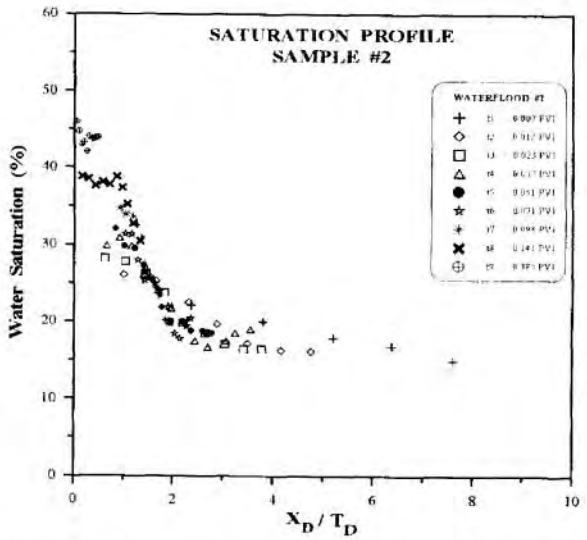


Figure 9 - Dimensionless response curve from the first waterflood on sample #2.

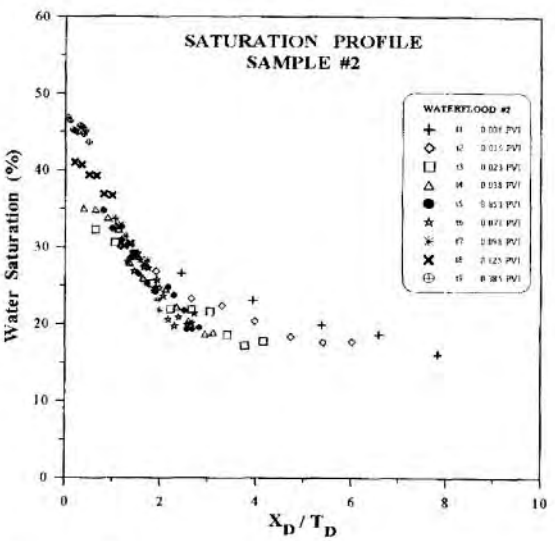


Figure 10-Dimensionless response curve from the second waterflood on sample #2.

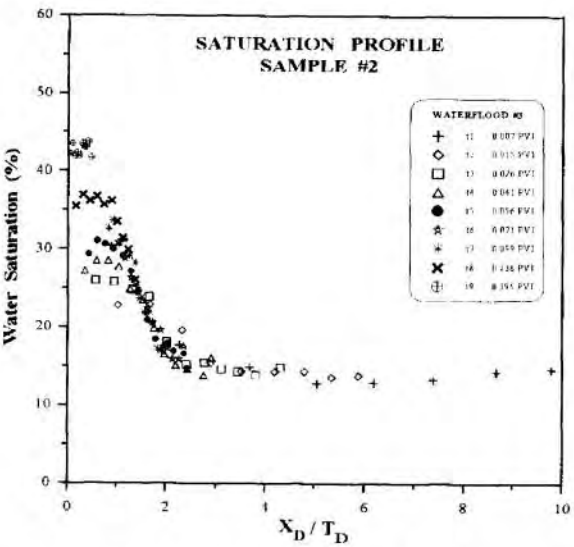


Figure 11 - Dimensionless response curve from the third waterflood on sample #2.

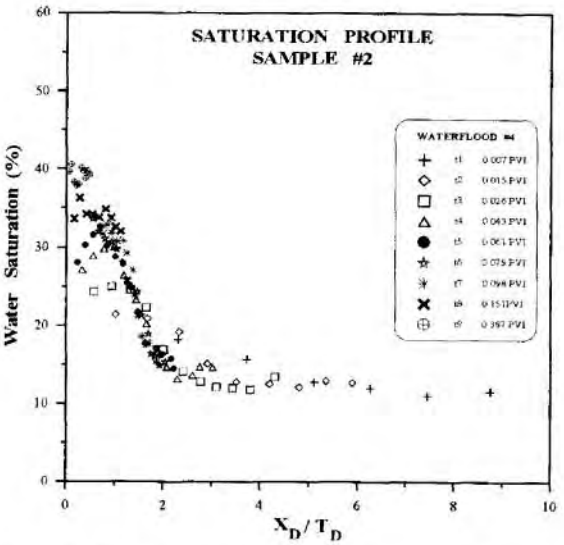


Figure 12 - Dimensionless response curve from the fourth waterflood on sample #2

Oil and water relative permeabilities were calculated from fluid production rates and differential pressure data acquired during the scanned experiments and computed according to the JBN method. Although this method is valid only for stable displacements the oil and water relative permeability curves were plotted just to verify their reproducibility. Figure 13 shows water relative permeabilities (Krw) as function of normalized water saturation (Sw*) from the eight waterfloods.

The existence of two distinct displacement mechanisms comes out by the sudden changing on the slope of the curves. Starting at the breakthrough, the produced water is derived from the fingering zone until the stable zone reaches the production face of the core what gives rise to that breaking on the slope of the curves. We can see that water relative permeabilities were not sensitive to the velocity of the displacing water but the extent of the fingering zone surely was. Figure 14 depicts both fingering zone

(slices 12 through 22) and the stable zone (slices 7 through 11) just before the breakthrough of the water phase during the second experiment on sample #2. The water saturation quickly increases at the fingering front (slices 22 back to 19) and remains practically constant backward the next 6 slices until the beginning of the stable zone (each zone = 10 mm).

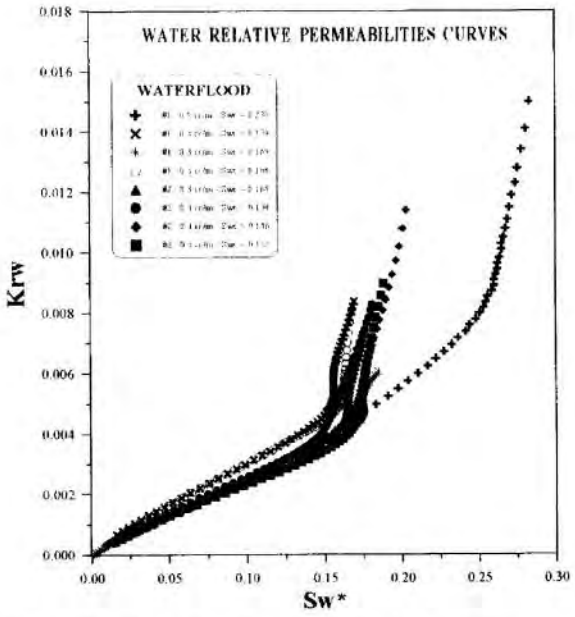


Figure 13 : Water relative permeability curves.

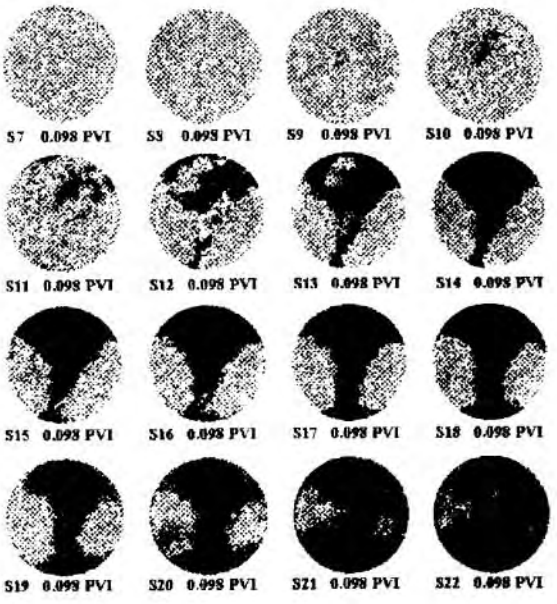


Figure 14 : CT images of both fingering and stable zone

The figure 15 shows the oil relative permeabilities as function of normalized water saturation. We noticed values of oil relative permeabilities greater then 1.0 , which has no physical meaning.

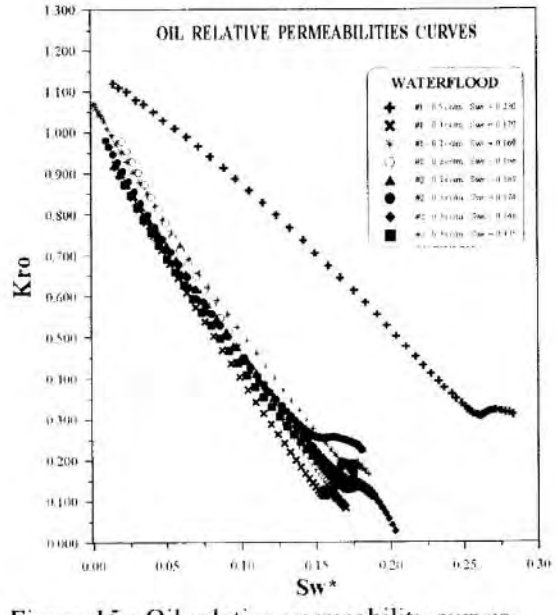


Figure 15 : Oil relative permeability curves.

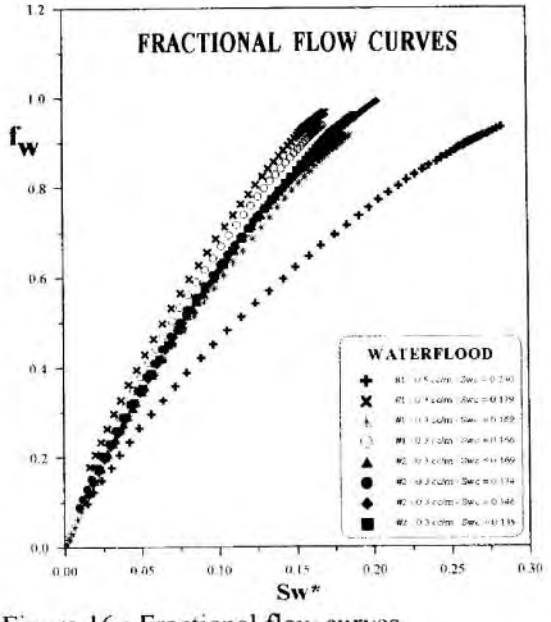


Figure 16 : Fractional flow curves.

The reason for such unreasonable values might be attributed to the characteristic poor fitting at the limits of the cumulative oil production curve what causes severe discrepancies to its derivatives around the breakthrough. Although the basic premiss of stable displacement has been broken, what may invalidate the magnitude of the oil relative permeability values themselves, we can realize that oil relative permeability is strongly influenced by the velocity of the injecting water. Thus, for a given water saturation, the higher the injection velocity, the higher the oil relative permeability. It suggests that the efficiency of a waterflood increases as the injecting fluid velocity becomes higher. Figure 13 and figure 15 shows that the oil and water relative permeability curves are likely to be reproducible provided displacements parameters be kept constant.

Figure 16 shows the fractional flow curves from the experiments. The shape of fractional flow curves is characteristic of a displacement dominated by fingering mechanisms. Their derivatives decreases continuously revealing that the water saturation increases smoothly showing no evidence of a shock front. We can see that the water fractional flow is also strongly affected by the velocity of the displacing fluid. Again, for a given water saturation, the higher the injection velocity, the lower the fractional flow. It suggests that the efficiency of a waterflood increases as the injecting water velocity also increases. It corroborates to the results obtained by the analysis of the oil relative permeability curves. Once again, for a given set of displacement condictions there is a strong likelihood of fractional flow curves be reproducible.

The figures 13, 15 and 16 show that the experiments carried out on sample #2 were more reproductive than those done on sample #1. It indicates that the use of solvents to clean the rock sample may have changed some properties of the porous media. In view of the fact that solvent extraction was not used in the resaturation process of sample #2, it may be undertake as a possible cause for the spreading of the relative permeability and fractional flow curves since these curves were much more closer for sample #2 than those for sample #1

## Conclusions

This study has demonstrated that CAT scanning is a useful tool for characterizing permeable media and visualizing the development of fingering throughout a core. Porosity and fluid saturation profiles can be directly determined from image data while image artifacts can be minimized through the use of computational methods of beam hardening correction. Many conclusions can be drawn from the results obtained in this study :

1- For a given set of displacement parameters, viscous fingering during unstable immiscible displacements in natural and consolidated porous media were very likely reproducible.
2- Even for a remarkably homogeneous natural and consolidated porous media, there is a strong likelihood of viscous fingering be a deterministical phenomenon instead of a statistical one. The fingering is subject to gravity forces and heterogeneities even of minimal magnitude.
3- Viscous fingering during unstable immiscible displacements in natural and consolidated porous media shall be a dimensionless self-similar process.
4- Oil relative permeability and fractional flow curves undergo strong influence of the velocity of injecting water while water relative permeabilty curves are not likely to.
5- The use of solvent extraction to clean the rock sample may alter some properties of the porous media.

## Notation

$$x_D = \frac{x}{L} \qquad t_D = \frac{|\vec{v}|\, t}{\Phi\, L} \qquad S_w^* = \frac{S_w - S_{wi}}{1 - S_{wi}}$$

## Nomenclature

| | |
|---|---|
| D | Core diameter |
| $f_{1D}$ | Dimensionless response function |
| $f_w$ | Fractional flow of water |
| k | Absolute permeability |
| $k_{ro}$ | Relative permeability to oil |
| $k_{rw}$ | Relative permeability to water |
| L | Length |
| M | Mobility ratio |
| P | Pressure |
| So | Oil saturation |
| Sor | Residual oil saturation |
| Sw | Water saturation |
| Sw* | Normalized water saturation |
| Swi | Connate water saturation |
| t | Time |
| $t_D$ | Dimensionless time |
| v | Superficial velocity |
| x | Distance from the inlet |
| $x_D$ | Dimensionless length |
| $\Psi$ | X-Ray attenuation coefficient |
| $\Phi$ | Porosity |
| $\mu$ | Viscosity |

## References


1. Sorbie, K.S., Tsibuklis, N.B. and Dwebi, A., Experimental testing of mobility predictions in averaged models of viscous fingering, Soc. Pet. Eng., 1991, 255-270.
2. Gupta, S. and Greenkorn, R.A., An experimental study of immiscible displacement with an unfavorable mobility ratio in porous media. Water Resources Research, 1974, vol. 10, No. 2 : 371-374
3. van Meurs, P. and van der Poel, C. A theoretical description of water drive processes involving viscous fingering, *Trans.*, AIME, 1957, vol. 213 : 103-112.
4. Chuoke, R.L.,van Meurs, P. and van der Poel, C. The instability of slow, immiscible, viscous liquid-liquid displacements in permeable media, *Trans.*, AIME, 1959, vol. 216 : 188-194.
5. Fayers, F.J. and Sheldon, J.W. The effect of capillary pressure and gravity on two-phase fluid in a porous medium. *Trans.*, AIME, 1958, vol. 216 : 147-155.
6. Moissis, D.E., Miller, C.A. and Wheeler, M.F., Simulation of miscible viscous fingering using a modified method of characteristics: Effects of gravity and heterogeneity., Soc. Pet. Eng. 1989 : 431-446.
7. Peters, E.J.,Afzal, N. and Gharbi, R. On scaling immiscible displacements in permeable media. J. Pet. Sci. Eng. 1993 : 183 - 205.
8. Peters, E.J. and Flock, D.L., The onset of instability during two-phase immiscible displacement in porous media., Soc. Pet. Eng. J. , 1981, 249-258.
9. Peters, E.J. and Hardham, W., Visualization of fluid displacements in porous media using computed tomography images, J. Pet. Sci. Eng. , 1990 : 155-168.
10. Holleben, C.R., Determinação de porosidade e saturações de fluidos através de tomografia computadorizada de Raios-X., Msc dissertation, Univ. Est. Campinas, São Paulo, 1993.
11. Silva, A.C., Analise de reprodutibilidade de digitações viscosas em meios porosos naturais consolidados., Msc dissertation, Univ. Est. Campinas, São Paulo, 1995.
12. Hove, A.O., Ringen, J.K. and Read, P.A., Visualization of laboratory corefloods with the aid of computerized tomography of X-Rays., SPE Res. Eng., 1987 : 148-154.
13. Peters, E.J., Broman, J.A. and Broman Jr., W.H., Computer image processing: A new tool for studying viscous fingering in corefloods.,SPE Res. Eng., 1987 : 720-728.
14. Wellington, S.L. and Vinegar,H.J., X-Ray computerized tomography., J. Pet. Tech., 1987 : 885-898.